KFUPM
Journal of Undergraduate Research International

Diamond Open Access 198

Article Petroleum Engineering

Effect of a Microbial Surfactant on the Surface Tension and Contact Angle in Hydrogen Geostorage

Abdulqader Hagash and Md Bashirul Haq*

Cite https://doi.org/10.64589/juri/231592

Submitted: April 23, 2026 Revised: May 07, 2026 Accepted: May 16, 2026

ABSTRACT

Understanding gas/brine interfacial tension (IFT) and rock wettability is essential for evaluating underground H_2 storage, particularly when a native or cushion gas is present and when the aqueous phase is modified to alter its interfacial behavior. This study investigates binary H_2/CH_4 mixtures at various pressures and temperatures to assess the effects of microbial-surfactant addition on IFT and static contact angles (CAs). CAs were measured on quartz (reservoir-side analogue) and Wolfcamp shale (seal-side analogue) using brine (Fluid 1, quartz and shale) and rhamnolipid-containing brine (Fluid 2; quartz only). Gas/brine IFT was measured for both fluids, and the resulting IFT and CA data were used to estimate static column-height support. All untreated systems exhibited water-wet to weakly water-wet characteristics (CA = 28°–55°). Thus, the wettability measurements primarily quantify changes in CA caused by gas composition and rhamnolipid addition and demonstrate how these changes interact with IFT in column-height calculations. Rhamnolipid addition consistently reduced IFT, but did not guarantee improved column-height support because the reduction in IFT often outweighed the beneficial reduction in CA. On quartz, Fluid 2 yielded lower estimated column heights than Fluid 1, indicating that surfactant-induced IFT reduction dominated the capillary response. Wolfcamp shale provided substantially higher capillary support than quartz, confirming its role as a more relevant seal-side basis for structural trapping assessment. These findings demonstrate that biosurfactant modification does not automatically enhance the static storage capacity and that reservoir- and seal-side substrates cannot be considered interchangeable in H_2 storage evaluations.

Keywords: underground H_2 storage; H_2/CH_4 mixtures; contact angle; interfacial tension; rhamnolipid; Wolfcamp shale; quartz; column height

1. INTRODUCTION

H_2 is often regarded as a key energy carrier in the transition to low-carbon energy systems. For large-scale and seasonal applications, underground H_2 storage in depleted reservoirs has emerged as a promising option because such formations offer established pore spaces, existing infrastructure, and a proven history of gas containment [1,2]. Under these conditions, however, H_2 is often mixed with CH_4 as a native reservoir gas or cushion component, rendering binary H_2/CH_4 systems directly relevant for storage assessment [1,3].

The interfacial behavior in depleted reservoirs plays a central role in controlling multiphase flow, phase distribution, capillary resistance, injectivity, and containment security. Therefore, wettability and gas/brine interfacial tension (IFT) are key parameters for evaluating gas retention and withdrawal performance [2,4]. Such assessments must consider both the storage interval and the sealing interval because the caprock governs the maximum gas column that can be supported beneath it by balancing capillary and buoyancy forces [5]. In this context, reservoir-side mineral and seal-side caprock responses should not be treated as interchangeable.

Previous studies on H_2/brine/quartz and H_2/brine/sandstone systems generally report water-wet to weakly water-wet behavior, although the absolute contact angles (CAs) and their pressure-temperature dependence vary with the substrate type, measurement method, and experimental protocol [6–8]. Studies on H_2/CH_4 systems relevant to depleted reservoirs show that mixed H_2/CH_4 systems can remain broadly water-wet, whereas IFT typically decreases as the CH_4 fraction and temperature increase [9,10]. These findings indicate that binary H_2/CH_4 behavior should not be inferred from pure-H_2 data alone when CH_4-bearing depleted reservoir conditions are of interest.

Recent studies have expanded the understanding of H_2-based gas mixtures for underground H_2 storage (Table 1). Alshammari et al. [11] investigated the influence of CH_4 and CO_2 as cushion gases on H_2/brine IFT and water/H_2/rock wettability, demonstrating that cushion-gas composition can affect the interfacial properties that control storage capacity, injectivity, and capillary sealing behavior. Al-Yaseri and Fatah [12] examined H_2/CH_4 exposure effects on sandstone and limestone pore structures, highlighting that H_2/CH_4 mixtures may influence rock/fluid interaction and pore-scale storage behavior. Earlier modeling work by Panfilov et al. [13] showed that $H_2/CO_2/CH_4$ underground storage involves coupled hydrodynamic, chemical, and microbial processes that can alter gas composition during storage. More recently, Tawil et al. [14] measured the solubility of H_2/CH_4

Published under an exclusive license by KFUPM

Table 1. *Summary of recent studies related to H_2-based gas mixtures in underground H_2 storage*

Study	Tested system and conditions	Main finding	Gap/Relevance
Alshammari et al. [11]	H_2/brine + CH_4/CO_2; MD; variable pressure–temperature–salinity.	Cushion gases affect IFT and wettability; CO_2 gives stronger IFT reduction.	Supports gas-composition effects; no rhamnolipid-modified H_2/CH_4 brine.
Al-Yaseri and Fatah [12]	H_2/CH_4 with sandstone and limestone; pore-structure study.	Mixed gas can influence pore-scale rock response.	Supports H_2/CH_4 testing, but not coupled CA–IFT–column-height analysis.
Panfilov et al. [13]	H_2 and H_2–CO_2–CH_4 storage; numerical modeling.	Flow, reaction, and microbial processes may alter stored-gas composition.	Shows mixture complexity; lacks direct laboratory CA/IFT data.
Tawil et al. [14]	H2/CH4 solubility in brine under underground hydrogen storage pressure–temperature conditions.	Gas composition controls dissolution and possible gas loss to brine.	Complements brine behavior; supports H_2/CH_4-specific tests.

mixtures in brine under underground H_2 storage conditions and showed that gas-mixture composition affects dissolution behavior in the aqueous phase. These studies confirm that H_2-based gas mixtures cannot be interpreted only from pure-H_2 systems because gas composition can influence interfacial behavior, pore-scale response, storage efficiency, and gas-loss mechanisms.

At present, most available studies focus on unmodified brines, conventional gas/brine/rock systems, pore-structure alterations, solubility, and numerical modeling. By contrast, limited attention has been given to brine systems modified by biosurfactants, particularly rhamnolipids, under binary H_2/CH_4 conditions. Therefore, the present study addresses this gap by linking rhamnolipid-induced changes in gas/brine IFT and quartz wettability to static column-height support.

Shale behavior is particularly important for seal analysis. Al-Mukainah et al. showed that H_2/brine/shale wettability and H_2/brine IFT are directly related to shale sealing efficiency and static H_2 column-height estimation [5]. Moreover, clean-surface studies on quartz demonstrate that CA measurements are highly sensitive to the surface preparation, roughness, and contamination history, which helps explain part of the spread among published datasets and underscores the need for careful interpretation of absolute CA magnitudes [7]. This issue is especially important when comparing results across different substrates and measurement campaigns.

Despite progress in the field, limited attention has been given to an integrated framework that combines a binary H_2/CH_4 system, a reservoir-side mineral analogue, a seal-side shale analogue, and aqueous-phase modification by biosurfactant addition within a single study [3]. In addition, biosurfactant-based fluid modification has not been sufficiently examined within a framework that directly links interfacial measurements to static seal-controlled column-height interpretations under binary H_2/CH_4 conditions [3]. These knowledge gaps are important because modifying the aqueous phase may change CA and IFT simultaneously, and these two shifts do not necessarily improve capillary support in the same direction. In other words, a lower CA alone does not guarantee a larger supported gas column if it is accompanied by a greater reduction in IFT.

Although the existing H_2/brine/rock wettability literature has established important baseline behavior for underground H_2 storage systems, most available studies have focused on conventional brines and unmodified aqueous phases. Previous work has examined H_2/brine/sandstone and H_2/brine/quartz wettability, H_2/CH_4 mixture wettability, and gas/brine IFT under different pressures, temperatures, salinities, and rock-surface conditions. These studies confirmed the importance of CA and IFT for H_2 containment and capillary trapping. However, the effect of microbial surfactants, particularly rhamnolipids, on coupled H_2/CH_4/brine/rock wettability and gas/brine IFT remains insufficiently explored. This gap must be addressed because biosurfactant addition can simultaneously reduce CA and IFT, and these two changes may have opposite effects on the estimated column height.

Accordingly, this study investigated binary H_2/CH_4 systems relevant to underground H_2 storage by treating quartz as a reservoir-side mineral analogue and Wolfcamp shale as a seal-side analogue. Static CA and gas/brine IFT were measured using a Krüss DSA100 high-pressure/high-temperature (HPHT) system with 3 wt.% NaCl brine (Fluid 1) as a baseline and a modified 3 wt.% NaCl brine solution containing 0.57 wt.% rhamnolipid biosurfactant (Fluid 2) at pressures ranging from 500 to 2000 psi and temperatures of 25 and 50 °C. Brine salinity was selected based on the stability of the biosurfactant at this concentration, and the biosurfactant concentration was adopted from the literature [15]. Fluid 2 was included to evaluate whether aqueous-phase modification could alter interfacial behavior in a way that changes the inferred static column height support. Therefore, the column-height interpretation adopted here is framed within a static capillary–buoyancy analysis rather than a dynamic flow model. The purpose of the wettability measurements in this study was to determine whether rhamnolipid addition and H_2/CH_4 composition cause measurable changes in CA and whether these changes improve or weaken the column-height response when combined with IFT.

2. METHODOLOGY

In this study, a Krüss DSA100 drop shape analyzer equipped with an optical high-pressure/high-temperature (HPHT) cell was used to quantify (i) the static CA of gas/brine/rock systems and (ii) the gas/brine IFT using pendant-drop analysis. Two aqueous fluids were examined: Fluid 1 (3 wt.% NaCl brine) and

Fluid 2 (3 wt.% NaCl brine + 0.57 wt.% rhamnolipid biosurfactant). Binary H_2/CH_4 mixtures were tested at 25 and 50 °C over pressures of 500–2000 psi. CAs were measured on quartz and Wolfcamp shale for Fluid 1 and on quartz for Fluid 2 (Table A2). The measured IFT and CA values were then used as inputs for subsequent capillary/column-height calculations.

2.1. Materials and Experimental Matrix. The same HPHT optical-cell workflow was applied for both the CA and IFT measurements, except that the CA measurements used a mounted rock/mineral substrate, whereas the IFT measurements used a free pendant droplet in the gas-filled cell. All measurements were processed using the Krüss acquisition/analysis software, which fitted the drop profile using Young–Laplace analysis to extract CA and IFT. The materials used in this study included NaCl (99.99 mol.%; Supelco/Merck, ACS, ISO, Reag. Ph Eur grade), laboratory-prepared deionized (DI) water with an electrical conductivity of 0.02 $\mu S \cdot cm^{-1}$ at 25 °C, and 0.57 wt.% rhamnolipid biosurfactant (supplier and purity not reported). H_2, CH_4, and N_2 gases were supplied by Air Liquide (99.99% purity; Saudi Arabia). Quartz and Wolfcamp shale were used as the reservoir- and seal-side substrates, respectively. Additional material details and the experimental matrix are provided in Tables A1 and A2 (Appendix A).

2.2. Sample Preparation and Cleaning Procedure.

2.2.1. Preparation of aqueous test fluids. Fluid 1 was gravimetrically prepared by dissolving NaCl (30 g) in DI water (1 L) and mixing for 24 h using a magnetic stirrer with a polytetrafluoroethylene (PTFE)-coated magnetic stir bar placed in the solution. A magnetic stir bar retriever was used to handle and remove the stir bars when required (Figures S1–S2). Mixing was continued until complete salt dissolution was achieved and the brine appeared visually homogeneous.

Fluid 2 was prepared as follows. Rhamnolipid was selected because it is a microbial biosurfactant with documented IFT reduction ability in petroleum-related applications. It was used in this study to evaluate whether rhamnolipid-modified brine can alter gas/brine IFT and quartz wettability under H_2/CH_4 storage conditions.

NaCl (30 g) and the rhamnolipid biosurfactant (5.7 g) were weighed and added to DI water to achieve a final solution mass of 1 kg. The mixture was magnetically stirred for 24 h using a PTFE-coated magnetic stir bar to ensure the full dispersion of the biosurfactant and complete homogenization of the brine phase. A magnetic stir bar retriever was used to handle the stir bars when necessary. Mixing was continued until the solution appeared visually homogeneous without persistent foaming, as shown in Figure S3.

Aqueous solutions were prepared using DI water, which has been reported in similar DSA100 studies to exhibit low electrical conductivity, thereby reducing uncertainty from dissolved impurities [16,17].

The pH and electrical conductivity of Fluid 2 were measured under ambient conditions to characterize its physicochemical properties prior to IFT testing and support the interpretation of its behavior in the subsequent CA and IFT measurements. Because Fluid 2 contains a rhamnolipid biosurfactant that exhibits pH-dependent ionization behavior and may influence adsorption at the solid–liquid interface, wettability, and IFT, knowledge of its pH is important. The pH of Fluid 2 was measured using a pH meter after rinsing the probe with DI water and immersing it directly into the fluid. The pH of the fluid was 6.32. Electrical conductivity was measured using a conductivity meter following the same probe-rinsing procedure and found to be 51.77 $mS \cdot cm^{-1}$.

2.2.2. Gas-mixture preparation (H_2 and CH_4). The H_2/CH_4 mixtures (H_2/CH_4 = 100%/0, 80%/20%, 60%/40%, 40%/60%, 20%/80%, 0/100%) were prepared in a dedicated gas mixture cell equipped with a calibrated pressure gauge. The gases were introduced sequentially by partial pressure following the ideal-gas partial-pressure mixing rule (Dalton's law), whereby the partial pressure of each component is directly proportional to its mole fraction in the final mixture [17]. The target composition was achieved at the desired total pressure by introducing the lower-fraction gas first, followed by the higher-fraction gas.

The pure gases were supplied directly from high-pressure cylinders without using a mixing cell.

2.3. Substrate Preparation and Conditioning. Quartz and Wolfcamp shale core samples were used as solid substrates. Wolfcamp shale was selected as a representative caprock sample. Prior to the CA measurements, each coupon was mounted on a custom holder inside the HPHT cell to provide a flat horizontal surface.

The two primary sources of error in the HPHT CA/IFT measurements were (i) contamination of the substrate and (ii) contamination within the wetted parts/equipment setup. Thus, steps were taken to minimize errors arising from these sources.

The substrates were cleaned using a plasma cleaner (Plasma Cleaner PDC-002-CE; 5 min air-plasma exposure) [18,19] (Figure S4) to remove surface impurities and organic contaminants [18–21]. Plasma cleaning was performed twice: once prior to the Fluid 1 campaign and once prior to the Fluid 2 campaign.

Following plasma cleaning, the coupons were immersed in Fluid 1 (quartz and Wolfcamp shale) and Fluid 2 (quartz only) for 24 h to ensure that the core samples were fully saturated with the respective fluids, thereby allowing the surfaces to equilibrate and reach stable conditions before the CA measurements. On the day of testing, the coupon was removed from the fluid and dried with N_2 gas immediately before droplet deposition until no visible surface moisture remained. Between consecutive experiments within the same fluid campaign, the coupon was re-immersed in the corresponding fluid for a few minutes while the next test was being prepared and subsequently re-dried with N_2 prior to reuse.

The quartz and Wolfcamp shale coupons (~2 cm × 2 cm × 0.5 cm) were cut from larger slabs and cleaned with deionized (DI) water. No additional solvents (e.g., toluene/acetone) were used to preserve their in situ surface properties. The substrates were prepared to maintain consistent surface characteristics for the wettability measurements without altering their natural properties.

2.4. Density Measurement.

2.4.1. Density inputs for Fluid 1. The brine density of 3 wt.% NaCl was obtained by first-order linear interpolation of the

available density data (2 and 5 wt.% NaCl) reported in the Supplementary Information [17] under the same pressure/temperature conditions. Direct density measurements were not performed for Fluid 1 because 3 wt.% NaCl is a simple brine system and reliable supplementary density data were available at nearby salinities. Because 3 wt.% lies between 2 and 5 wt.%, linear interpolation was considered appropriate. The interpolated 3 wt.% brine density values used in the calculations are provided in Table A3 (Appendix A).

2.4.2. Density inputs for Fluid 2. Density measurements were conducted using an Anton Paar SVM series viscometer–densimeter equipped with an integrated Peltier temperature control [22], as shown in Figure S5 (a). Prior to each run, the measurement cell was rinsed with distilled water and, when necessary, with a suitable cleaning solution to remove any residual material from the previous measurements. The instrument was then adjusted to the required test temperature (25 or 50 °C) and pressure and allowed to stabilize before sample loading. The prepared solution was transferred into a clean 5 mL syringe, ensuring that no air bubbles were present [23].

The syringe was connected to the instrument inlet, and the sample was injected slowly and continuously until liquid emerged from the outlet tubing (Figure S5 (b)), confirming complete filling of the measuring cell. The measurement was initiated and the instrument was operated until the final density reading was displayed and recorded. The density of Fluid 2 is provided in Table A4 (Appendix A).

2.4.3. Gas density calculation procedure. The density of H_2 and CH_4 gases, both as pure components and as mixtures, was determined using two online thermodynamic property databases to ensure reproducibility. The densities of pure H_2 and CH_4 were obtained from the NIST Chemistry WebBook (National Institute of Standards and Technology, USA) [24]. The densities of the H_2/CH_4 gas mixtures were calculated using the FLUIDAT® on the Net database (FDT Software & Consulting GmbH) [25].

The gas densities for both pure gases and gas mixtures are compiled in Tables A5–A7 (Appendix A), and all IFT and CA values reported in this work are based on the corrected density differences using Tables A3–A7.

2.5. Apparatus Configuration. The experimental system consisted of a Krüss DSA100 drop shape analyzer integrated with an optical HPHT measurement cell, a high-performance camera, and an LED lighting source. The HPHT cell was connected to a gas-mixture cell via an ISCO syringe pump for pressurization and mixture injection. A dedicated gas-mixture cell with a pressure gauge was used to prepare and deliver the H_2/CH_4 mixtures, while a manual dosage/pressure unit was used to generate and control droplets at the needle tip during the CA/IFT measurements.

The DSA100 HPHT system is rated up to ~10,000 psi and ~200 °C; the present experiments were conducted within pressures of 500–2000 psi and temperatures of 25 and 50 °C.

2.6. Cleaning Procedure and Run Sequencing. Before commencing the experiments, the HPHT cell and wetted parts were inspected for residual oil from previous users. If oil residue was present, acetone and toluene were used to thoroughly clean the components and remove organic contaminants. If no oil residue was observed, the components were directly rinsed with DI water.

Before each experiment, the gas lines were purged with the gas mixture to be used to ensure that the lines were fully filled with the desired gas composition and to eliminate any residual gases from previous experiments, thereby guaranteeing accurate and contamination-free gas delivery.

After each experiment, the HPHT chamber was depressurized and the gas mixture was vented/purged. The HPHT cell was purged with the metering valve closed to prevent backflow contamination of the gas-mixture flow lines, and the brine-flow line section was rinsed with DI water before replacing the brine for subsequent experiments.

2.7. Contact-angle Measurements. Static CAs were measured using the sessile-drop method [27] according to ASTM D5946. Only static CAs were measured in this study; advancing and receding CAs were not measured because of the experimental scope and HPHT operational constraints. Prior to each measurement, the cleaned and dried substrate (quartz or Wolfcamp shale) was mounted on a custom-designed holder inside the HPHT chamber (Figure 1 (e)). The substrate was carefully aligned to provide a horizontal surface because accurate droplet-profile analysis requires the droplet baseline to remain parallel to the reference plane during Young–Laplace fitting.

After substrate mounting, the chamber was sealed, and the temperature was adjusted to 25 or 50 °C (Figure 1 (h)). The selected gas system, including pure H_2, pure CH_4, and the H_2/CH_4 mixtures, was then introduced into the chamber using an ISCO syringe pump (Figure 1 (i)) connected to the gas-mixture cell (Figure 1 (j)). The pressure was increased to the required value between 500 and 2000 psi in 500 psi increments.

Before droplet deposition, the fluid was withdrawn from the liquid dosage unit (Figure 1 (d)) by rotating the control wheel until the maximum suction was achieved. Once the desired volume was drawn, the liquid dosage unit was closed, and the needle valve was opened. The system was allowed to equilibrate for approximately 5 min to minimize mass-transfer effects and stabilize the measurement environment. A small droplet was first formed at the needle tip, after which a sessile droplet of the test fluid (Fluid 1 or Fluid 2) was deposited on the dry substrate surface. The droplets were completely released from the needle. The droplet profile was recorded using the instrument's integrated high-performance camera, and the static CA was automatically calculated by the DSA software using Young–Laplace fitting.

Final experimental conditions were reported from a successful, stable run. After droplet deposition, the CA was continuously monitored using the DSA software and was not taken from the initial transient response. Equilibrium was considered achieved when the droplet profile became stable and the CA trend reached a stable plateau after the equilibration period. The reported CA was obtained by averaging this stable plateau region, and the standard deviation within this interval was used to assess the stability of the in-run measurements. The runs affected by droplet asymmetry, noticeable vibration, pressure drift, or leakage were rejected and repeated until a stable plateau was attained.

2.8. Interfacial-tension Measurements. Gas/brine IFT measurements were conducted using the pendant-drop

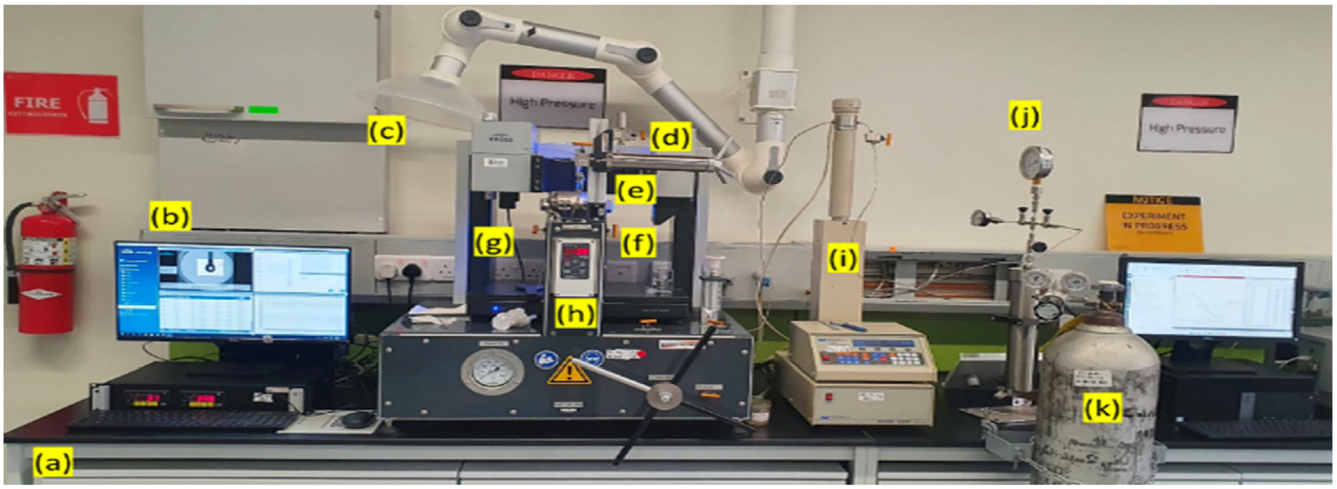

Figure 1. Photograph of the Krüss DSA100 HPHT experimental setup used for the gas/brine CA and IFT measurements: (a) anti-vibration table, (b) data acquisition computer, (c) gas venting unit, (d) liquid dosage unit, (e) HPHT measurement cell with camera and LED light, (f) gas-mixture inlet from the ISCO syringe pump, (g) gas-mixture outlet, (h) temperature-control knob, (i) ISCO syringe pump, (j) gas-mixture cell with pressure gauge, and (k) dry N_2 gas cylinder for cleaning[26]

technique coupled with Young–Laplace fitting[28,29]. The same cleaning protocol used for the CA experiments was followed before each IFT measurement. After cleaning, the HPHT chamber was sealed (Figure 1(e)), and the temperature was maintained at 25 or 50 °C (Figure 1 (h), depending on the experimental condition. Once the desired volume was drawn, the liquid dosage unit was closed, the needle valve was opened, and a pendant droplet of the aqueous test fluid was formed at the tip of the capillary needle inside the chamber. Because biosurfactant addition increased the density of Fluid 2, a slightly smaller droplet volume was required to preserve a stable pendant shape. Accordingly, the droplet volume was adjusted to 16 ±1.5 μL for Fluid 1 and 15 ±1.5 μL for Fluid 2.

After droplet formation, the gas phase was introduced into the chamber using an ISCO syringe pump (Figure 1 (i)) until the target pressure (500, 1000, 1500, or 2000 psi) was reached. As gas diffusion progressed, the dynamic IFT gradually decreased until the droplet approached equilibrium with the surrounding gas phase. The DSA100 software continuously monitored the IFT, and the equilibrium value was identified when no further measurable changes in the IFT were observed. The equilibrium IFT was averaged over a stable time interval of approximately 250–350 s after stabilization to improve reliability. This plateau-based averaging approach ensured that the reported IFT represented a stable equilibrium value, rather than an initial transient reading.

3. RESULTS AND DISCUSSION

This section describes two property-based blocks. For each property, the experimental observations are interpreted and the mechanisms responsible for the measured trends are identified. Literature comparisons were used to support and contextualize the present findings. The data in this study were compared with the literature data presented in Table B1 (Appendix B).

3.1. Interfacial Tension.

3.1.1. Benchmarking against published data and analysis of magnitude differences. The IFT measurements of the gas mixtures agreed well with the published data (Figures 2 (a) and 2 (b)) and decreased with increasing pressure. The present IFT results showed that the gas/brine interface clearly responded to gas composition, temperature, and fluid chemistry. For Fluid 1, IFT generally decreased as the CH_4 fraction and temperature increased. This finding indicates that CH_4 enrichment and higher temperatures reduce the resistance at the gas/brine interface. The effect of temperature can be explained by increases in molecular motion and weaker cohesive forces at the gas/brine interface. The CH_4 effect reflects the different interfacial behavior of CH_4-rich mixtures compared with H_2-rich mixtures.

An exact match in magnitude was not expected because the benchmark study did not use gas mixtures with an identical composition. Specifically, the present study used H_2/CH_4 mixtures at temperatures of 25 and 50 °C with 3 wt.% of NaCl, whereas Muhammed et al. investigated $H_2/N_2/CH_4/CO_2$ mixtures at temperatures from 30 to 70 °C with 2–20% NaCl. Because the current binary mixture contains only H_2 and CH_4 and does not contain N_2 or CO_2, direct quantitative agreement with the published multicomponent gas-mixture data is not expected. A comparison between the pure gas and published data also validates the current IFT data, as demonstrated in Figures 2 (c) and 2(d). In both cases, pure H_2 exhibited a higher IFT than pure CH_4, and both values decreased as the temperature increased.

The most probable reason for the slightly lower IFT lower values obtained in the current study compared with those reported in the literature is the use of different salinity ranges and pressure–temperature conditions. For markedly lower IFT values, the most probable cause are lower temperatures or differences in the gas-composition window.

Overall, the present IFT results agree with the literature in terms of trend, particularly the decrease in IFT with increasing pressure, temperature, and CH4 fraction. Differences in the absolute IFT values are expected because the present work employed a binary H2/CH4 system with 3 wt.% NaCl, whereas the benchmark studies used different gas compositions, salinities, and pressure–temperature windows.

3.1.2. Comparative responses of Fluid 1 and Fluid 2. Direct comparison of Fluid 1 and Fluid 2 showed that the

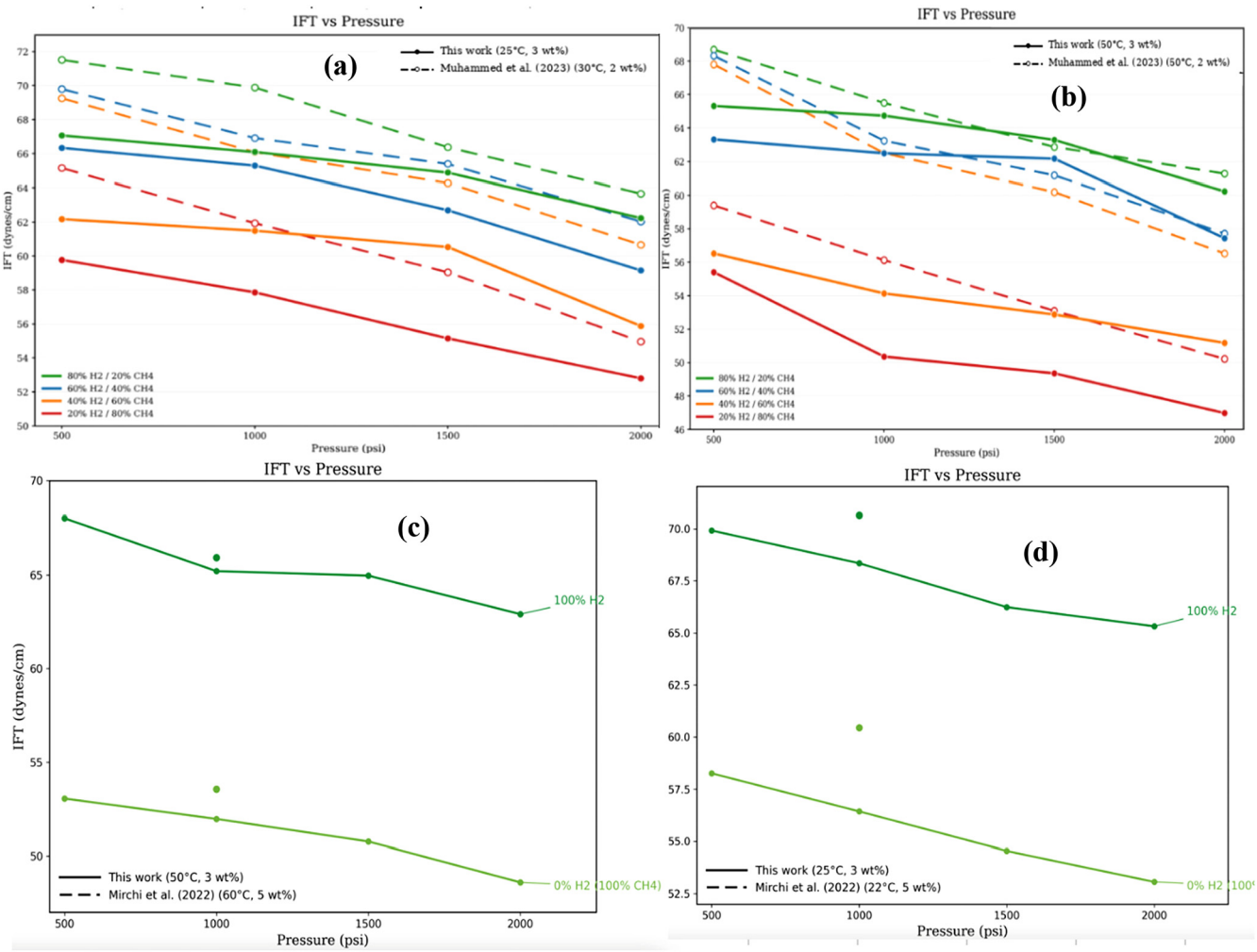

Figure 2. Comparison of the measured gas/brine IFT data with published reference data as a function of pressure (500–2000 psi at 500 psi increments with 3 wt.% NaCl brine): (a) H_2/CH_4 mixtures at 25 °C vs. Muhammed et al.[17] at 30 °C and 2 wt.% NaCl, (b) H_2/CH_4 mixtures at 50 °C vs. Muhammed et al[17] at 50 °C and 2 wt.% NaCl, (c) pure H_2 and pure CH_4 at 50 °C vs. Mirchi et al[30] at 60 °C and 5 wt.% NaCl, and (d) pure H_2 and pure CH_4 at 25 °C vs. Mirchi et al.[30] at 22 °C and 5 wt.% NaCl

surfactant strongly influenced IFT, as shown in Figures 3 (a) and 3 (b). Similar to Fluid 1, the IFT measurements in Fluid 2 decreased with increasing pressure, CH_4 fraction, and temperature; however, the values measured for Fluid 2 were generally lower than those measured for Fluid 1.

Mechanistically, the lower IFT values observed for Fluid 2 can be attributed to rhamnolipid adsorption at the gas/brine interface. The hydrophilic portion of the rhamnolipid molecule interacts with the aqueous phase, whereas the hydrophobic portion is oriented toward the gas phase. This arrangement reduces the interfacial free energy, thereby explaining the lower IFT values obtained (for) Fluid 2. Thus, the IFT data provide a clearer and more direct indication of rhamnolipid action at the gas/brine interface than the CA data, which are also influenced by local solid-surface conditions.

3.2. Contact Angle.

3.2.1. Benchmarking against published data and analysis of magnitude differences. The CA measurements show that all tested systems remained water-wet to weakly water-wet. This behavior is consistent with the expected initial wettability of untreated quartz and shale substrates because no oil-aging or gas-wetting treatment was applied. Therefore, rather than simply identifying the wetting classification, the CA results clarify the direction and magnitude of CA changes caused by gas composition and rhamnolipid addition, and how these changes contribute to the column-height calculations.

For Fluid 1, the CAs measured on quartz and Wolfcamp shale showed some scatter with increasing pressure and temperature; however, the overall wetting state remained consistent. This finding suggests that pressure was not the dominant factor controlling CA within the tested range. Instead, the CA response appears to be controlled by the combined effects of gas composition, substrate type, and surface conditions.

The quartz CA values fell within the water-wet to weakly water-wet range, but they were generally higher than the published data (Figures 4 (a)–4 (d)). Therefore, the comparison reveals agreement in the overall water-wet to weakly water-wet classification, although not necessarily in the absolute CA magnitude.

The observed scattering can be attributed to several experimental and surface-related factors. Unlike IFT, CA depends on

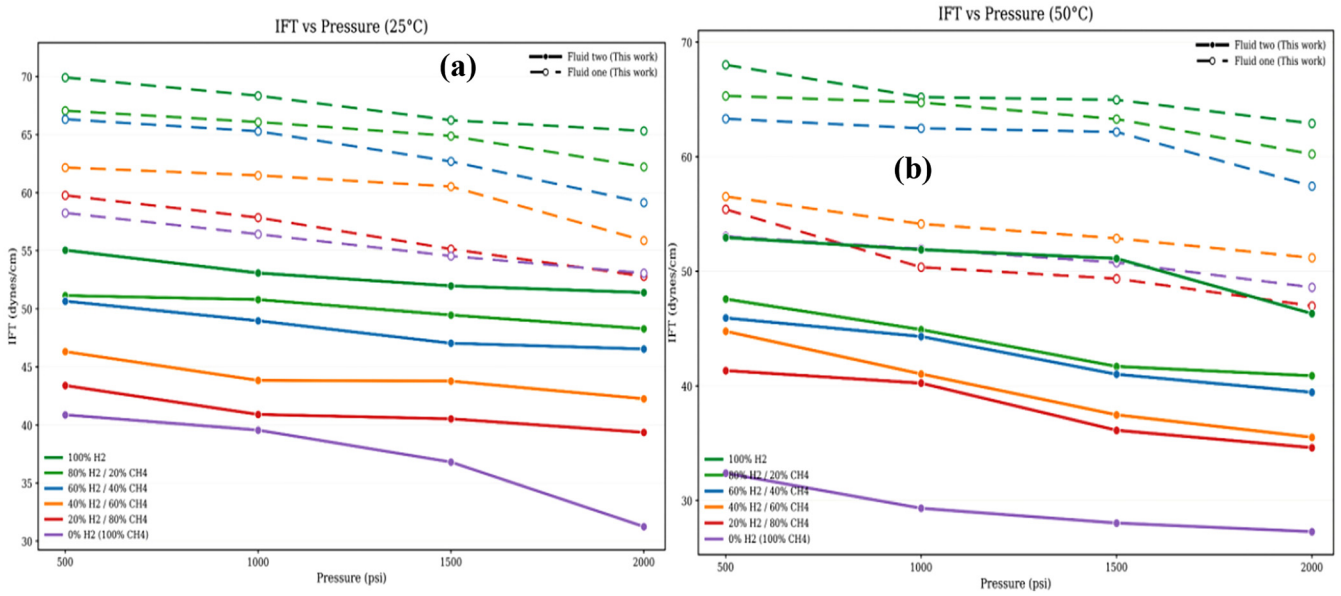

Figure 3. Comparison of gas/brine IFT values between Fluid 1 (solid lines) and Fluid 2 (dashed lines) as a function of pressure: (a) at 25 °C and (b) at 50 °C

a three-phase interaction among the gas, brine, and solid surface. Therefore, small differences in surface roughness, drying history, residual moisture, and droplet-baseline selection can produce noticeable scatter, even when the overall wettability classification remains unchanged.

Several factors may explain the offset between the present quartz data and published values. First, the current binary H_2/CH_4 system does not have the same composition as the $H_2/CH_4/N_2/CO_2$ mixtures reported by Muhammed et al. Thus, the present binary H_2/CH_4 system differs compositionally from the $H_2/CH_4/N_2/CO_2$ systems reported by Muhammed et al., and these compositional differences may contribute to the observed differences in CA. Second, the pressure–temperature–salinity windows were not identical because the current study used temperatures of 25 and 50 °C with 3 wt.% NaCl, whereas the literature covered different temperature and salinity ranges. Third, comparisons with the data reported by Hashemi et al. should be interpreted carefully because that study used different substrates and measurement methods. Specifically, Hashemi et al. used a captive-bubble approach on Bentheimer sandstone, whereas the present study used sessile-drop measurements on quartz. Differences in quartz surface conditions may also partially explain the remaining offset.

Overall, the observed differences did not affect the main trends in the present dataset. The directional behavior remained physically consistent, even if the absolute values differed from those reported in some published analogues. Therefore, the literature observations provide contextual support rather than the primary explanation for the present data. Importantly, Muhammed et al. used sessile-drop measurements on quartz; therefore, the differences between their study and the present work cannot be attributed solely to the measurement method.

Previous clean-quartz studies[31,32] demonstrated that CA on quartz is highly sensitive to the cleaning method. The CA of very clean surfaces may be very small, even approaching 0°. Therefore, the effect of rigorous surface preparation on lowering CA may be greater than the effects of temperature, pressure, and salinity within the studied range.

The higher CAs observed in the present measurements with Fluid 1 compared with certain published values may also be attributed to differences in surface conditions, N_2 drying time, CH_4 fraction in the gas mixture, and the pressure–temperature–salinity window. Pressure did not appear to be the dominant factor controlling CA within the tested range. Instead, the CA response was more strongly influenced by local surface conditions, drying history, residual moisture, and droplet-baseline selection. These factors can introduce scattering and mask simple monotonic pressure trends.

However, the overall wetting classification was consistent with the expected behavior of the untreated substrates. Because this classification serves as a baseline in the present study, the primary value of the experiments lies in quantifying the direction and magnitude of the CA changes and their contribution to the column-height calculation.

Wolfcamp shale showed a distinct seal-side wettability response compared with quartz. Although the measured values were scattered, the shale data remained within the water-wet to weakly water-wet range, supporting its use as a caprock-side substrate in column-height interpretation. For all three comparisons of Wolfcamp shale, the literature data were consistently higher than the present measurements, as shown in Figure 5.

This finding may be explained by differences in surface-condition history. For instance, Al-Mukainah et al. measured CAs on Wolfcamp shale at 50 °C and 14.7–1000 psi with 10 wt.% NaCl. In addition, the samples were cleaned with pure N_2 gas, whereas plasma cleaning was not specified. This observation further supports the interpretation that CAs are highly sensitive to surface condition. Thus, the differences in CA values may be attributed primarily to differences in surface state. Salinity may also contribute to the observed differences because the present study used 3 wt.%. NaCl, whereas the reference study used 10

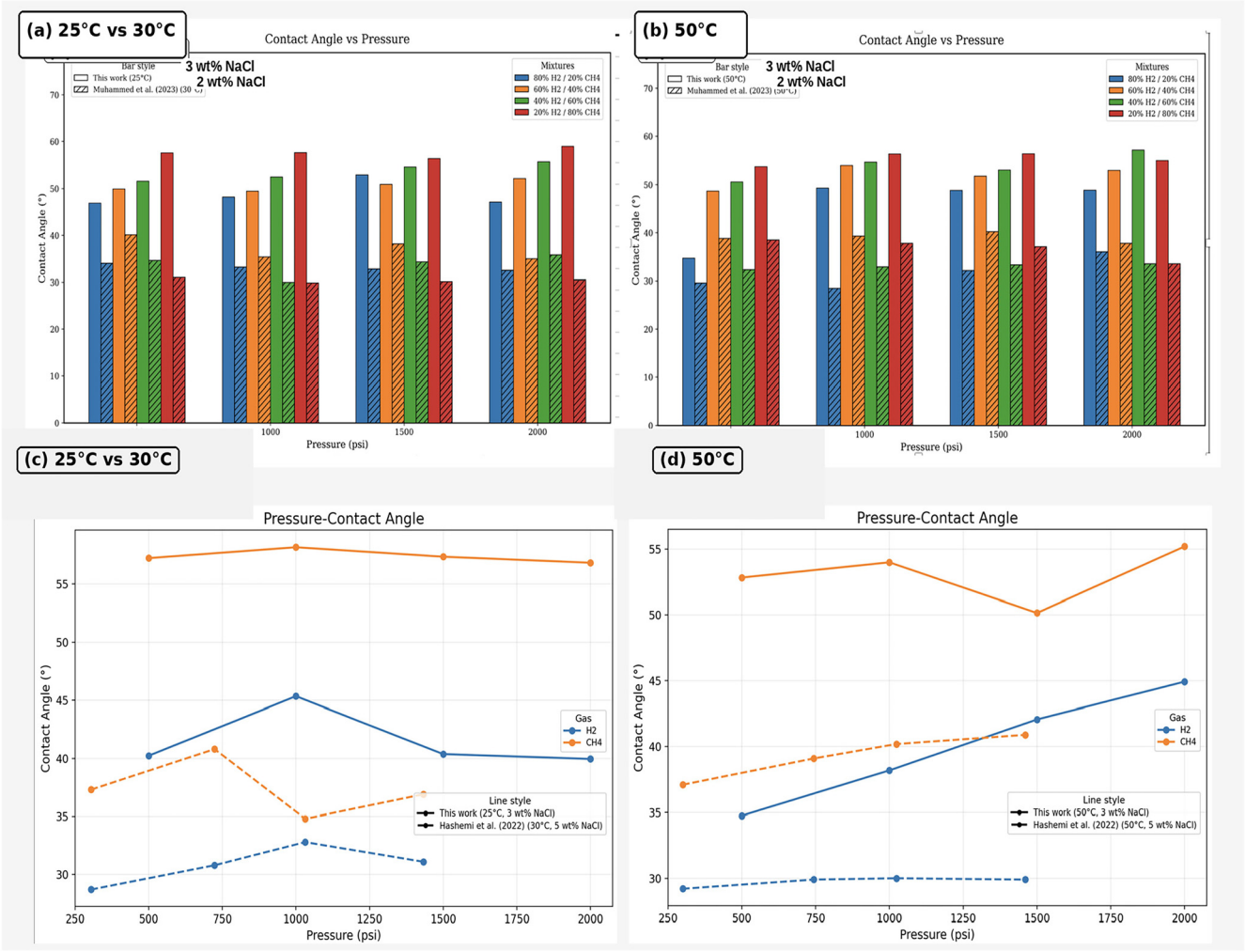

Figure 4. Comparison of the quartz CA data (measured in 3 wt.% NaCl brine over 500–2000 psi) with published reference data as a function of pressure: (a) H_2/CH_4 mixtures at 25 °C vs. Muhammed et.al.[17] at 30 °C and 2 wt.% NaCl, (b) H_2/CH_4 mixtures at 50 °C vs. Muhammed et al.[17] at 50 °C and 2 wt.% NaCl, (c) pure H_2 and CH_4 vs. Hashemi et al[33] at 30 °C and 3 wt.% NaCl over approximately 270–1450 psi, and (d) pure H_2 and pure CH_4 vs. Hashemi et al.[33] at 50 °C and 3 wt.% NaCl over approximately 270–1450 psi

wt.% NaCl. However, the salinity effect is likely to be smaller than the surface-condition effect.

The Wolfcamp shale dataset was physically consistent. Although the individual curves did not show strictly monotonic pressure or temperature trends, the overall dataset exhibited pressure-dependent variations and temperature-dependent shifts in CA across the gas-mixture (Figures 6 (a) and 6 (b)). Thus, the dataset preserves the intrinsic trend while retaining realistic experimental scatter. The higher values reported in the literature may be attributed to differences in surface conditioning and brine salinity rather than to fundamentally different wetting behaviors.

3.2.2. Comparative responses of Fluid 1 and Fluid 2 and implications of rhamnolipid addition. Rhamnolipid addition (Fluid 2) generally lowered the quartz CAs relative to those measured in Fluid 1, indicating a shift toward more water-wet conditions (Figures 7 (a) and 7 (b)). Although the system remained within the expected water-wet to weakly water-wet range, the rhamnolipid-modified brine produced a measurable CA shift on quartz. This shift is important because column height depends on both CA and IFT. Therefore, even a wettability change that does not alter the overall wetting class can influence the calculated capillary support. The reduction was generally more evident at 50 °C and in CH_4-rich cases, whereas some 25 °C conditions showed smaller or less systematic changes. The CA response was more scattered than the IFT response because wettability depends on both the gas–brine interface and local quartz surface conditions, including cleanliness, drying consistency, and possible surfactant adsorption on the solid surface.

Overall, the results suggest that the rhamnolipid-modified brine shifts the quartz CA toward lower values, although the magnitude of this shift is sensitive to surface conditions. This wettability interpretation applies only to quartz because shale was not tested with Fluid 2.

3.3. Effect on Column Height. The column-height analysis provides a clear link between the measured IFT and CA data. The key finding is that a lower CA alone does not guarantee higher capillary support because the simultaneous reduction in IFT exerts a stronger effect on the final column-height estimate.

In this study, static column height was interpreted within a structural-trapping framework in which gas retention beneath the

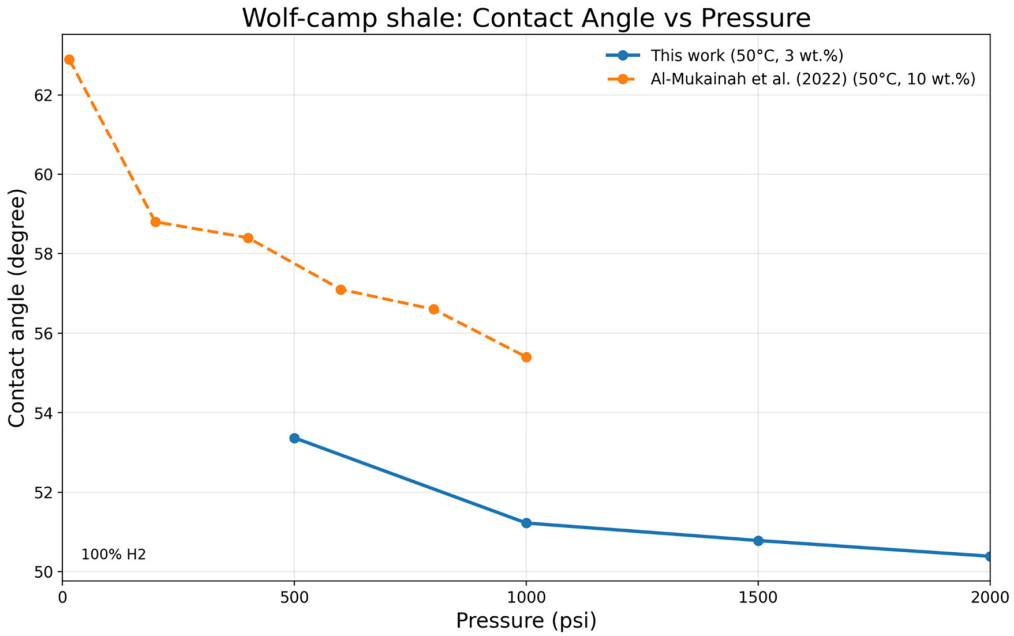

Figure 5. Comparison of the present Wolfcamp shale CA data for pure H_2 with published data from Al-Mukainah et al.

caprock was controlled by the balance between capillary resistance and buoyancy. Therefore, the discussion is anchored to the sealing system rather than the storage substrate.

In the present context, Wolfcamp shale provides the most direct basis for interpretation because the estimated column height depends on the measured IFT, CA, density difference, and characteristic pore-throat radius governing capillary entry. This seal-centered approach maintains consistency with the physical meaning of both the seal-only and seal-reservoir formulations used to interpret static trapping behavior.

The governing capillary–buoyancy relationship is described by Eq. 1:

$$h_seal = \frac{2\gamma \cos\theta}{g\,\Delta\rho\, r_{seal}} \quad (1)$$

where h_seal represents the maximum height supported by the seal alone, γ represents the measured IFT, θ is the measured CA, $\Delta\rho$ is the density difference between the coexisting phases, g is the gravitational acceleration, and r represents the average pore radius of the caprock, assumed to be 50 nm[35,36] for shale caprock and 2 μm[36] for quartz. Within the reference framework adopted from the source material, the seal radius was treated as a nanoscale caprock property, whereas the reservoir radius was introduced in the combined formulation to account for the capillary contributions of both the seal and storage interval.

3.3.1. Comparative responses of quartz and shale in Fluid 1. Figure 8 shows that Wolfcamp shale consistently exhibited significantly higher estimated column heights than quartz at

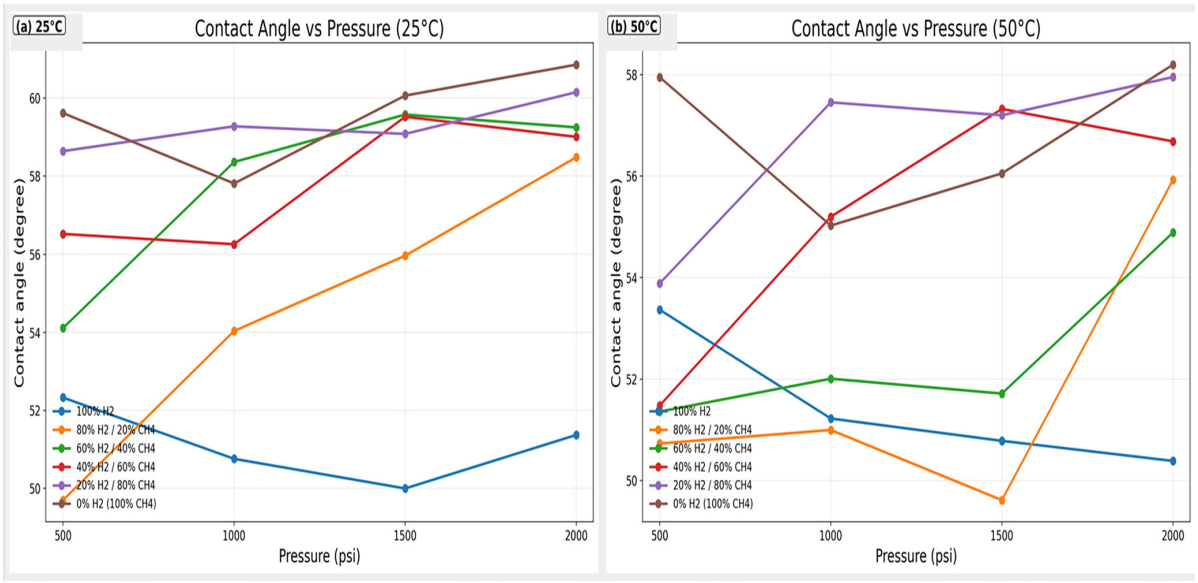

Figure 6. Contact angles measured on Wolfcamp shale with Fluid 1 as a function of pressure (3 wt.% NaCl brine over 500–2000 psi at 500 psi increments) at (a) 25 °C and (b) 50 °C

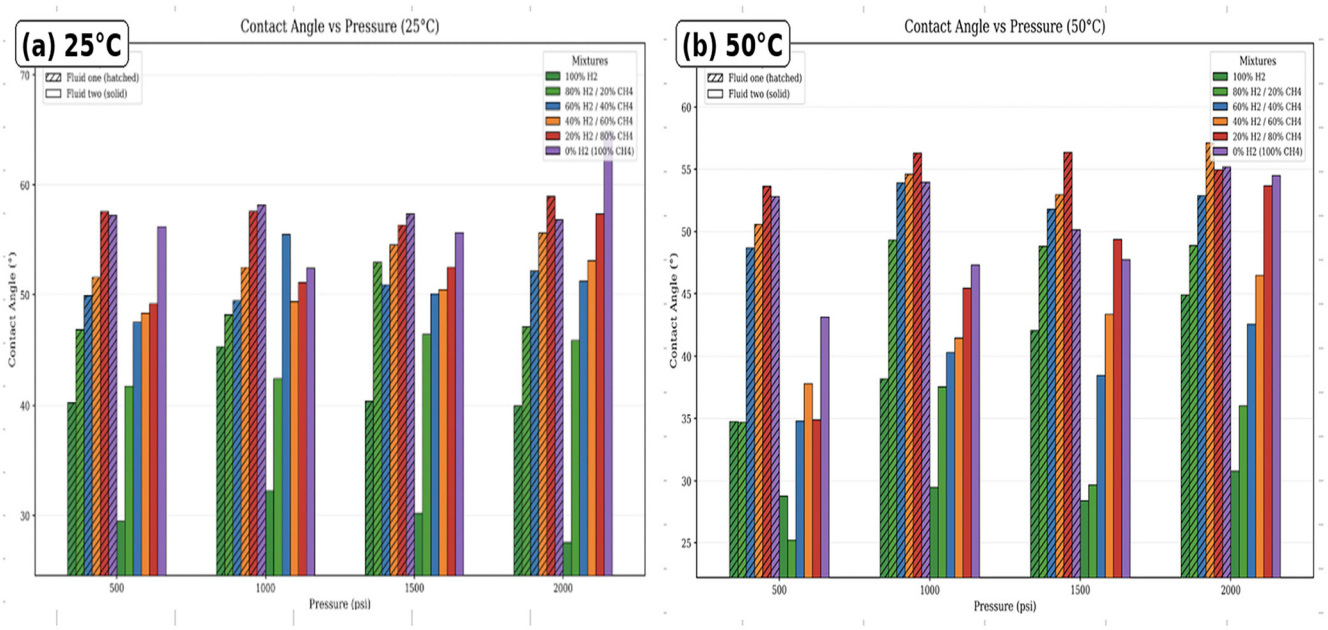

Figure 7. Comparison of quartz CA responses between Fluid 1 (solid bars) and Fluid 2 (dashed bars) as a function of pressure at (a) 25 °C and (b) 50 °C

25 and 50 °C in Fluid 1. This substantial difference does not imply that quartz acts as a seal; rather, it reflects the strong influence of the pore-throat radius in the column-height equation. Specifically, the capillary term is strongly affected by IFT, CA, density difference, and, most importantly, pore-throat radius. Accordingly, shale was used as the seal-side material for evaluation, whereas quartz served as a comparative substrate.

Increasing the CH_4 content generally reduced the estimated column height, although the pressure response was not monotonic. This nonmonotonic behavior is mainly inherited from scatter in the measurements because the IFT exhibits a clear pressure-dependent decrease. Because column height depends on IFT, CA, and the density difference, small variations in CA can affect the calculated capillary terms. Despite this scatter, Wolfcamp shale consistently provided higher estimated column heights than quartz at both temperatures. Therefore, containment and storage interpretations should focus primarily on Wolfcamp shale, with quartz serving to demonstrate substrate dependence.

3.3.2. Comparative responses of Fluid 1 and Fluid 2 on quartz. As shown in Figure 9, Fluid 2 produced lower estimated column heights than Fluid 1 at both 25 °C (Figure 9 (a)) and 50 °C (Figure 9 (b)) for all tested gas compositions. This result agrees with the measured IFT and CA data. Although Fluid 2 reduced the quartz CA, which would normally favor stronger capillary trapping, it also markedly reduced the IFT. Because column height depends strongly on IFT, the reduction in IFT became the dominant effect and lowered the estimated column height on quartz.

The difference between Fluid 1 and Fluid 2 was in the CH_4-rich cases. The pressure trend was not perfectly monotonic, mainly because the column height was calculated using several inputs, including IFT, CA, and density difference. Because CA measurements exhibit some scatter, small variations in CA can affect the calculated column-height response even when the IFT trend is clearer.

This result also demonstrates why CA classification alone is insufficient. Although the quartz system remained water-wet to weakly water-wet, the measured changes in IFT and CA produced different column-height responses. Thus, the significance of this experiment lies in quantifying the coupled IFT–CA effect rather than simply assigning a wetting category.

The quartz results showed that rhamnolipid addition did not improve the estimated column-height support in this study. Instead, the reduction in IFT outweighed the benefit of a lower CA. Because Fluid 2 was not tested on Wolfcamp shale, this finding should not be interpreted as a direct conclusion regarding caprock sealing behavior. Rather, it should be considered a quartz-based indication of how rhamnolipid-modified brine affects the system.

Overall, the results should be interpreted within the scope of controlled static laboratory measurements. The quartz-based column-height calculation was used only to compare Fluid 1 and Fluid 2 under identical surface conditions. It should not be interpreted as a real caprock sealing-capacity estimate because quartz is not a representative sealing material. Wolfcamp shale is a more relevant seal-side rock. In addition, the column-height model is a simplified static calculation based on capillary and buoyancy forces. Therefore, it does not fully represent real reservoir conditions, where heterogeneity, fractures, capillary hysteresis, dynamic injection and withdrawal processes, and time-dependent fluid–rock interactions may affect sealing performance.

4. CONCLUSIONS

This study examined gas/brine IFTs, static CAs, and the resulting column-height implications for binary H_2/CH_4 systems using 3

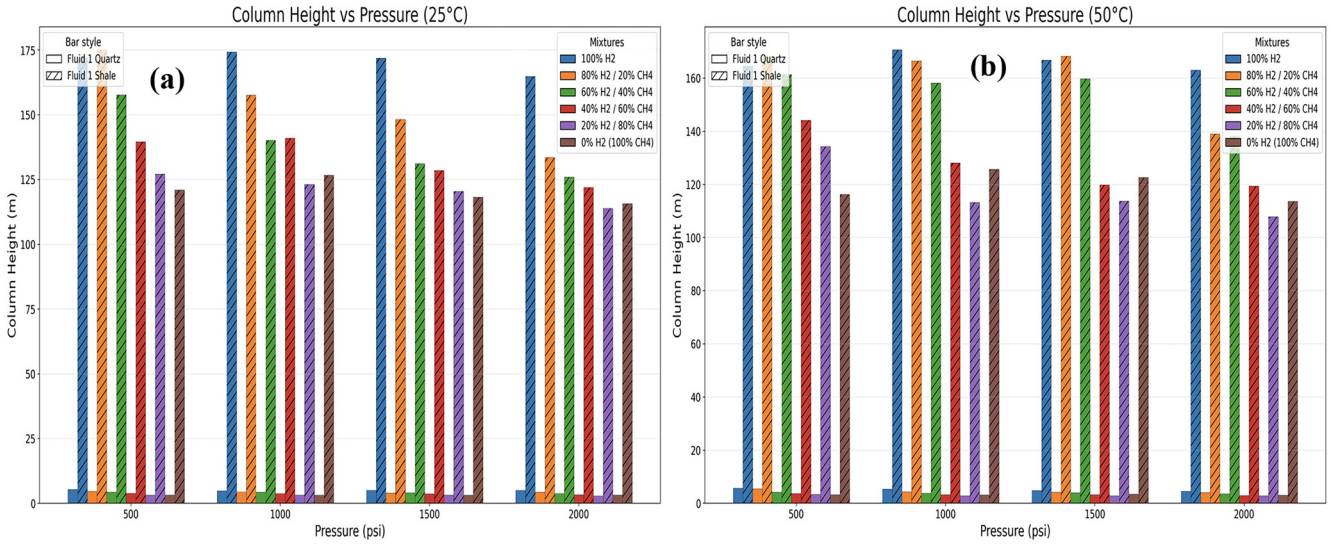

Figure 8. Comparison of estimated column heights between Wolfcamp shale (dashed bars) and quartz (solid bars) in Fluid 1 (3 wt.% NaCl brine) as a function of pressure at (a) 25 °C and (b) 50 °C

wt.% NaCl (Fluid 1) and 3 wt.% NaCl + 0.57 wt.% rhamnolipid biosurfactant (Fluid 2) at 500–2000 psi and 25–50 °C. The Kruss DSA100-HPHT workflow provided a coherent experimental basis for quantifying both gas/brine IFT and rock wettability across the investigated H_2/CH_4 compositions. Fluid 1 was evaluated on both quartz and Wolfcamp shale, whereas Fluid 2 was evaluated on quartz only. Based on the experimental results and comparative analyses presented in this study, the following conclusions can be drawn:

(1) The IFT dataset showed strong agreement with published analogue studies. In the present system, IFT decreased with increasing pressure, temperature, and CH_4 fraction. The differences in absolute IFT values relative to the literature data were mainly attributable to differences in gas composition and experimental conditions.

(2) The CA dataset remained within a water-wet to weakly water-wet framework, consistent with the expected behavior of untreated quartz and shale substrates in the absence of oil-aging or gas-wetting treatments. Although some absolute CA values differed from those reported in the literature, the directional behavior remained physically consistent and robust. The observed offsets were plausibly related to surface-state history, cleaning procedures, and gas composition. Therefore, the primary significance of the CA results lies in quantifying the magnitude and direction of wettability changes caused by gas composition and

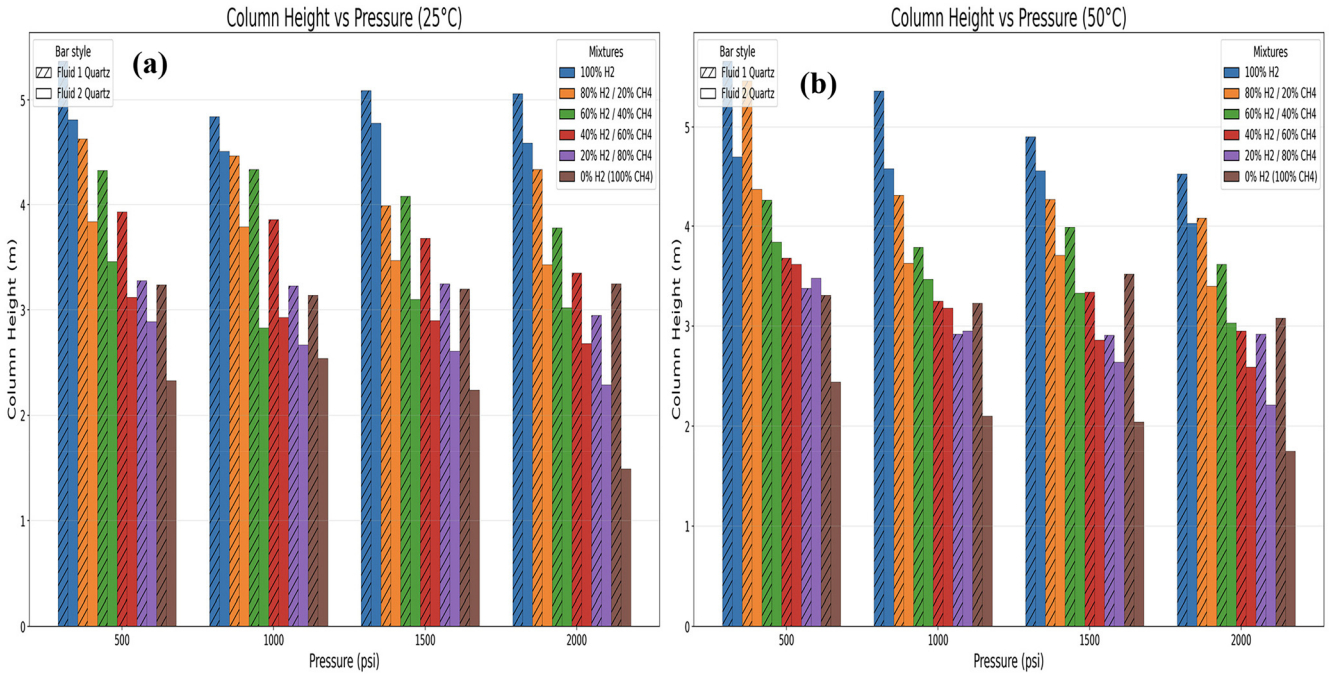

Figure 9. Comparison of estimated column heights between Fluid 1) (dashed bars) and Fluid 2 (solid bars) for quartz as a function of pressure at (a) 25 °C and (b) 50 °C

rhamnolipid addition, rather than in identifying the water-wet classification itself.

(3) In Fluid 1, Wolfcamp shale provided the primary seal-controlled reference for column-height interpretation and generally yielded greater capillary support than quartz, supporting its suitability as a caprock analogue for structural-trapping assessment. The addition of rhamnolipid to Fluid 2 consistently reduced IFT, shifting the quartz response toward lower IFT values across the investigated pressure and composition ranges, while also generally reducing quartz CAs.

(4) For quartz, the net effect of Fluid 2 relative to Fluid 1 was a reduction in the estimated column height. Although lower CA values in Fluid 2 would be expected to increase capillary support, the stronger and more systematic reduction in IFT dominated the response and therefore reduced the inferred column-height capacity. This conclusion is based on quartz as the common comparison substrate between Fluid 1 and Fluid 2. Because Fluid 2 was not tested on Wolfcamp shale, the effect of rhamnolipid on shale sealing behavior remains indirect and should be verified through future measurements using Fluid 2 on shale. This finding confirms that column-height behavior is governed by the coupled effect of IFT and CA and that changes in CA can be important even when the overall wetting class remains unchanged.

5. RECOMMENDATIONS

Based on the experimental limitations and interpretations developed in this study, the following recommendations are proposed to strengthen future work and improve the robustness of storage-capacity assessments:

(1) Extend Fluid 2 measurements to Wolfcamp shale so that the surfactant effect on the actual caprock/seal can be evaluated directly rather than inferred solely from quartz behavior.

(2) Adopt a more systematically documented surface-conditioning protocol, including repeated cleaning verification and surface-roughness documentation before each experimental campaign, to address the high sensitivity of absolute CA values to surface conditions.

(3) Increase the number of repeat measurements and explicitly report uncertainty ranges, particularly for CA measurements, because this property is sensitive to substrate surface conditions, cleaning history, drying consistency, and droplet-baseline selection.

(4) Quantify how uncertainties in CA and IFT propagate into the calculated column-height values. A more consistent surface-conditioning protocol, including plasma cleaning before each run measurement and controlled N_2 drying times, is also recommended to reduce CA scatter.

(5) Include advancing and receding CA measurements to better quantify wettability hysteresis and provide a more representative assessment of dynamic wettability under gas injection and withdrawal conditions.

AFFILIATIONS AND AUTHOR DETAILS

Undergraduate Author

Abdulqader Hagash – *Department of Petroleum Engineering, King Fahd University of Petroleum and Minerals (KFUPM), 31261, Dhahran, Saudi Arabia*; 0009-0005-7250-6152
Email: s202272520@kfupm.edu.sa ;

Corresponding Author

Md Bashirul Haq – *Research Mentor, Department of Petroleum Engineering, King Fahd University of Petroleum and Minerals (KFUPM), 31261, Dhahran, Saudi Arabia*; 0000-0003-1414-9976
Email: bhaq@kfupm.edu.sa

REFERENCES

(1) Hassan, Q., Algburi, S., Sameen, A. Z., Jaszczur, M. & Salman, H. M. Hydrogen as an energy carrier: properties, storage methods, challenges, and future implications. *Environ. Syst. Decis.* **44**, 327–350 (2024).

(2) Muhammed, N. S. *et al.* Hydrogen storage in depleted gas reservoirs: A comprehensive review. *Fuel* **337**, 127032 (2023).

(3) Muhammed, N. S., Haq, B. & Al Shehri, D. Role of methane as a cushion gas for hydrogen storage in depleted gas reservoirs. *Int. J. Hydrog. Energy* **48**, 29663–29681 (2023).

(4) Aslannezhad, M. *et al.* A review of hydrogen/rock/brine interaction: Implications for Hydrogen Geo-storage. *Prog. Energy Combust. Sci.* **95**, 101066 (2023).

(5) Al-Mukainah, H., Al-Yaseri, A., Yekeen, N., Hamad, J. A. & Mahmoud, M. Wettability of shale–brine–H2system and H2-brine for assessment of the sealing capacities of shale formations during underground hydrogen storage. *Energy Rep.* **8**, 8830–8843 (2022).

(6) Hashemi, L., Glerum, W., Farajzadeh, R. & Hajibeygi, H. Contact angle measurement for hydrogen/brine/sandstone system using captive-bubble method relevant for underground hydrogen storage. *Adv. Water Resour.* **154**, 103964 (2021).

(7) Al-Yaseri, A., Abdel-Azeim, S. & Al-Hamad, J. Wettability of water-H2-quartz and water-H2-calcite experiment and molecular dynamics simulations: Critical assessment. *Int. J. Hydrog. Energy* **48**, 34897–34905 (2023).

(8) Higgs, S. *et al.* In-situ hydrogen wettability characterisation for underground hydrogen storage. *Int. J. Hydrog. Energy* **47**, 13062–13075 (2022).

(9) Mirchi, V., Dejam, M. & Alvarado, V. Interfacial tension and contact angle measurements for hydrogen-methane mixtures/brine/oil-wet rocks at reservoir conditions. *Int. J. Hydrog. Energy* **47**, 34963–34975 (2022).

(10) Hashemi, L., Boon, M., Glerum, W., Farajzadeh, R. & Hajibeygi, H. A comparative study for H 2 –CH 4 mixture wettability in sandstone porous rocks relevant to underground hydrogen storage. *Adv. Water Resour.* **163**, 104165 (2022).

(11) Alshammari, S., Abdel-Azeim, S., Al-Yaseri, A. & Qasim, A. The Influence of CH_4 and CO_2 on the Interfacial Tension of H_2 –Brine, Water–H_2 –Rock Wettability, and Their Implications on Geological Hydrogen Storage. *Energy Fuels* **38**, 15834–15847 (2024).

(12) Al-Yaseri, A. & Fatah, A. Impact of H2-CH4 mixture on pore structure of sandstone and limestone formations relevant to subsurface hydrogen storage. *Fuel* **358**, 130192 (2024).

(13) Panfilov, M., Gravier, G. & Fillacier, S. Underground Storage of H2 and H2-CO2-CH4 Mixtures. in *ECMOR X - 10th European Conference on the Mathematics of Oil Recovery* (European Association of Geoscientists & Engineers, Amsterdam, Netherlands, 2006). doi:10.3997/2214-4609.201402474.

(14) Tawil, M. *et al.* Solubility of H2-CH4 mixtures in brine at underground hydrogen storage thermodynamic conditions. *Front. Energy Res.* **12**, 1356491 (2024).

(15) Awadh, M. *et al.* Machine Learning and Kinetic Insights into Biomass and Biosurfactant Production for Enhanced Oil Recovery Applications. *SPE J.* **31**, 1915–1931 (2026).
(16) Turkoglu, S. *et al.* Dynamic Wetting Properties of Silica-Poly (Acrylic Acid) Superhydrophilic Coatings. *Polymers* **15**, 1242 (2023).
(17) Muhammed, N. S., Haq, B. & Al Shehri, D. Role of methane as a cushion gas for hydrogen storage in depleted gas reservoirs. *Int. J. Hydrog. Energy* **48**, 29663–29681 (2023).
(18) Al-Yaseri, A., Wolff-Boenisch, D., Fauziah, C. A. & Iglauer, S. Hydrogen wettability of clays: Implications for underground hydrogen storage. *Int. J. Hydrog. Energy* **46**, 34356–34361 (2021).
(19) Hosseini, M., Fahimpour, J., Ali, M., Keshavarz, A. & Iglauer, S. Capillary Sealing Efficiency Analysis of Caprocks: Implication for Hydrogen Geological Storage. *Energy Fuels* **36**, 4065–4075 (2022).
(20) Iglauer, S., Salamah, A., Sarmadivaleh, M., Liu, K. & Phan, C. Contamination of silica surfaces: Impact on water–CO2–quartz and glass contact angle measurements. *Int. J. Greenh. Gas Control* **22**, 325–328 (2014).
(21) D20 Committee. Test Method for Corona-Treated Polymer Films Using Water Contact Angle Measurements. doi:10.1520/D5946-17.
(22) Anton Paar. Kinematic Viscometer: SVM Author: Anton Paar. (n.d.).
(23) D02 Committee. Test Method for Density, Relative Density, and API Gravity of Liquids by Digital Density Meter. doi:10.1520/D4052-11.
(24) Linstrom, P. NIST Chemistry WebBook, NIST Standard Reference Database 69. National Institute of Standards and Technology https://doi.org/10.18434/T4D303 (1997).
(25) Bronkhorst High-Tech B.V. FLUIDAT®on the Net. Bronkhorst Repository Location: https://www.fluidat.com/ (n.d.).
(26) Muhammed, N. S., Haq, B. & Al Shehri, D. CO2 rich cushion gas for hydrogen storage in depleted gas reservoirs: Insight on contact angle and surface tension. *Int. J. Hydrog. Energy* **50**, 1281–1301 (2024).
(27) Muhammed, N. S. *et al.* A review on underground hydrogen storage: Insight into geological sites, influencing factors and future outlook. *Energy Rep.* **8**, 461–499 (2022).
(28) Mouallem, J. *et al.* Critical review and meta-analysis of the interfacial tension of CO2-brine and H2-brine systems: Implications for CO_2 and H_2 geo-storage. *Fuel* **356**, 129575 (2024).
(29) Aslannezhad, M. *et al.* A review of hydrogen/rock/brine interaction: Implications for Hydrogen Geo-storage. *Prog. Energy Combust. Sci.* **95**, 101066 (2023).
(30) Mirchi, V., Dejam, M. & Alvarado, V. Interfacial tension and contact angle measurements for hydrogen-methane mixtures/brine/oil-wet rocks at reservoir conditions. *Int. J. Hydrog. Energy* **47**, 34963–34975 (2022).
(31) Al-Yaseri, A., Abdel-Azeim, S. & Al-Hamad, J. Wettability of water-H2-quartz and water-H2-calcite experiment and molecular dynamics simulations: Critical assessment. *Int. J. Hydrog. Energy* **48**, 34897–34905 (2023).
(32) Ali, M. *et al.* Hydrogen wettability of quartz substrates exposed to organic acids; Implications for hydrogen geo-storage in sandstone reservoirs. *J. Pet. Sci. Eng.* **207**, 109081 (2021).
(33) Hashemi, L., Boon, M., Glerum, W., Farajzadeh, R. & Hajibeygi, H. A comparative study for H 2 –CH 4 mixture wettability in sandstone porous rocks relevant to underground hydrogen storage. *Adv. Water Resour.* **163**, 104165 (2022).
(34) Al-Mukainah, H., Al-Yaseri, A., Yekeen, N., Hamad, J. A. & Mahmoud, M. Wettability of shale–brine–H2system and H2-brine interfacial tension for assessment of the sealing capacities of shale formations during underground hydrogen storage. *Energy Rep.* **8**, 8830–8843 (2022).
(35) Iglauer, S., Pentland, C. H. & Busch, A. CO_2 wettability of seal and reservoir rocks and the implications for carbon geo-sequestration. *Water Resour. Res.* **51**, 729–774 (2015).
(36) Nelson, P. H. Pore-throat sizes in sandstones, tight sandstones, and shales. *AAPG Bull.* **93**, 329–340 (2009).

Appendix A.

This appendix includes the essential supporting tables used for the experimental description and column-height calculations, including material information, the experimental matrix, and density inputs.

Appendix B.

Table A1. *Chemicals, substrates, and key equipment used in this study*

Item	Type/Phase	Description	Supplier/Purity
NaCl	Solid	NaCl used to prepare 3 wt.% brine	Supelco (Merck)/ACS, ISO, Reag. Ph Eur grade/99.99 mol%
Deionized water	Liquid	Base water for all aqueous solutions	Laboratory-prepared DI water/Electrical conductivity = 0.02 $\mu S \cdot cm^{-1}$ at 25 °C
Rhamnolipid	Solid/Liquid	Rhamnolipid biosurfactant added to Fluid 2 at 0.57 wt.%	Not recorded
H_2	Gas	Gas phase component	Air Liquide, Saudi Arabia / 99.99%
CH_4	Gas	Gas phase component	Air Liquide, Saudi Arabia / 99.99%
N_2	Gas	Used for drying/cleaning and flushing as needed	Air Liquide, Saudi Arabia / 99.99%
Quartz	Solid	Substrate for CA (Fluid 1 and Fluid 2)	Not recorded
Wolfcamp shale	Solid	Substrate for CA (Fluid 1 only)	Wolfcamp shale (user-specified)

Table A2. *Experimental matrix*

Fluid type	Test Case	Gas phase mixtures (%)		Salinity (wt.%)	Temperature (°C)	Pressure (psi)
		H_2	CH_4			
Fluid 1 (3 wt.% NaCl)	Case 1	100	0	3	25, 50	500–2000
	Case 2	80	20	3	25, 50	500–2000
	Case 3	60	40	3	25, 50	500–2000
	Case 4	40	60	3	25, 50	500–2000
	Case 5	20	80	3	25, 50	500–2000
	Case 6	0	100	3	25, 50	500–2000
Fluid 2 (3 wt.% NaCl + 0.57 wt.% rhamnolipid biosurfactant)	Case 1	100	0	3	25, 50	500–2000
	Case 2	80	20	3	25, 50	500–2000
	Case 3	60	40	3	25, 50	500–2000
	Case 4	40	60	3	25, 50	500–2000
	Case 5	20	80	3	25, 50	500–2000
	Case 6	0	100	3	25, 50	500 - 2000

Table A3. *Density ($kg \cdot m^{-3}$) of 3 wt.% NaCl brine used in the calculations (user-provided)*

Pressure (psi)	25 °C	50 °C
500	1016.330	1009.096
1000	1017.003	1010.350
1500	1017.810	1011.620
2000	1019.083	1012.753

Table A4. *Density ($kg \cdot m^{-3}$) of Fluid 2 (3 wt.% NaCl + 0.57 wt.% rhamnolipid biosurfactant) used in the calculations*

Pressure (psi)	25 °C	50 °C
14.7	1017.9	1005.5
500	1019.0	1010.2
1000	1020.3	1011.4
1500	1021.6	1012.8
2000	1022.8	1015.3

Table A5. *Density ($kg \cdot m^{-3}$ at 25 °C) of pure H_2 and CH_4 gases used in the calculations (user-provided).*

Mixture	500 psi	1000 psi	1500 psi	2000 psi
100% H_2	2.747	5.385	7.918	10.35
100% CH_4	23.68	50.15	78.92	108.5

Table A6. *Density ($kg \cdot m^{-3}$ at 25 °C) of H_2/CH_4 gas mixtures used in the calculations (user-provided).*

Mixture	500 psi	1000 psi	1500 psi	2000 psi
100% H_2/0% CH_4	2.747	5.385	7.918	10.35
80% H_2/20% CH_4	6.636	13.07	19.26	25.16
60% H_2/40% CH_4	10.58	20.97	31.03	40.68
40% H_2/60% CH_4	14.65	29.37	43.9	57.97
20% H_2/80% CH_4	18.95	38.76	58.95	78.91
0% H_2/100% CH_4	23.68	50.15	78.92	108.5

Table A7. *Density ($kg \cdot m^{-3}$ at 50 °C) of H_2/CH_4 gas mixtures used in the calculations (user-provided)*

Mixture	500 psi	1000 psi	1500 psi	2000 psi
100% H_2/0% CH_4	2.538	4.979	7.329	9.591
80% H_2/20% CH_4	6.121	12.06	17.78	23.25
60% H_2/40% CH_4	9.737	19.28	28.52	37.39
40% H_2/60% CH_4	13.45	26.85	40.02	52.77
20% H_2/80% CH_4	17.32	35.1	52.98	70.68
0% H_2/100% CH_4	21.48	44.65	69.05	93.82

Table B1. *Benchmark data*

Study	Property	System	Experimental conditions	Purpose
Muhammed et al. (2023)	Quartz CA and gas-brine ST for mixed gases	$H_2/CH_4/CO_2/N_2$/brine/quartz	500–3000 psi; 30–70 °C; 2–20 wt.% NaCl	Primary mixed-gas benchmark
Hashemi et al. (2022)	Contact angle (CA)	H_2/CH_4/brine/Bentheimer sandstone	30 and 50 °C; 20–100 bar; pure water and 5000 ppm NaCl	Supporting wettability benchmark
Mirchi et al. (2022)	Pure-gas IFT endpoints	H_2/CH_4/brine system	1000 psi; 22–60 °C; ~2 wt.% NaCl	Support for pure-gas IFT ordering and temperature response